Appl Nanosci (2013) 3:49–55
DOI 10.1007/s13204-012-0067-y

ORIGINAL ARTICLE

Synthesis of ZnO/Al:ZnO nanomaterial: structural and band gap variation in ZnO nanomaterial by Al doping

Muhammad Nafees · Wasim Liaqut · Salamat Ali · Muhammad Ahsan Shafique

Received: 8 December 2011 / Accepted: 10 February 2012 / Published online: 28 February 2012

Abstract Pure ZnO and Al-doped ZnO nanomaterial have been successfully fabricated using zinc acetate dihydrate in a basic aqueous solution of KOH through solution precipitation method then treated at 600°C in air. The XRD analysis confirms the Wurtzite hexagonal crystal structure of the product with crystallite size in 32–53 nm range. The morphology of the product has been studied under scanning electron microscopy (SEM). The simultaneous differential scanning calorimetry and thermogravimetric analyses were used to investigate thermal decomposition temperature and different phase transitions up to 800°C. The optical properties and variation in band gap of ZnO by Al doping were investigated by ultraviolet–visible spectroscopy.

Keywords ZnO · Band gap · Nanomaterial · Lattice strain · Al doping

Introduction

ZnO nanomaterials are extensively used in many applications, which have attracted much attention in the present years. Bulk ZnO have a direct band gap of 3.37 eV (at bulk state) and a larger exciton binding energy (60 meV). The electronic band gap of ZnO has been predicted theoretically and calculated by many people (Oshikiri and Aryasetiawan 2000; Muscat et al. 2001; Usuda and Hamada 2002; Uddin and Scuseria 2006; Shishkin and Kresse 2007; Christoph Friedrich et al. 2011; Dixit et al. 2011; Yan et al. 2011), and lot of experimental work have been done to find out the band gap of ZnO (varying 2.9–3.7 eV) (Alhamed and Abdullah 2010; Ma et al. 2011; Sakthivelu et al. 2011; Zandi et al. 2011; Tan et al. 2005; Bandyopadhyay et al. 2002; Inamdar et al. 2007; Ananthakumar et al. 2010). ZnO is very useful in several opto-electronic field such as optical sensors and light emitters (RF Service 1997; Makino et al. 2000), etc. In addition, ZnO is also very useful in gas detecting devices and piezoelectric application (Fortunato et al. 2005; Gong et al. 2006; Song et al. 2006; Jeong et al. 2003; Zhang et al. 2006). In fact, many application and devices having bulk ZnO, and ZnO nanomaterial have been established (Ma et al. 2011; R.F. Service 1997; Makino et al. 2000; Fortunato et al. 2005; Gong et al. 2006; Song et al. 2006; Jeong et al. 2003; Zhang et al. 2006; Yu et al. 2006).

There are many methods to synthesize ZnO nanomaterial such as, preparation by sputtering (Yan et al. 2011), chemical vapor deposition (Park et al. 2006), molecular beam epitaxy (MBE) (Fons et al. 2006), spry pyrolysis (Joseph et al. 1999), laser deposition (Chen et al. 2005), and the soft chemical method (Ristic et al. 2005; Kuo et al. 2006). Alhamed and Abdullah (2010) has discussed structural and optical properties of ZnO:Al films prepared by the sol–gel method. The solution precipitation method is predominantly gorgeous because of its simplicity, low costs, and obtained product of good crystalline quality, which makes it superior to the other methods. Here, we report a very simple solution precipitation method to synthesize ZnO nanomaterial and Al-doped ZnO with different doping concentration (3, 5, and 10%) to study the effect of doping concentration on structural and optical properties.

M. Nafees (✉) · W. Liaqut · S. Ali · M. A. Shafique
Material/Nano-Science Research Lab (MNRL),
Department of Physics, GC University,
Lahore, Pakistan
e-mail: Rajvi_gcu@yahoo.com

Table 1 Reaction scheme for synthesis

$Zn(CH_3CO_2)_2{\cdot}2H_2O + AlOH(CH_3CO_2)_2 + KOH$	$Zn(CH_3CO_2)_2{\cdot}2H_2O + KOH$
↓ Stirring	↓ Stirring
$xZn(OH)_2 + 1{-}xAl(OH)_3$	$Zn(OH)_2$
↓ 600°C	↓ 600°C
$Zn_x\ Al_{1-x}\ O + H_2O$	$ZnO + H_2O$

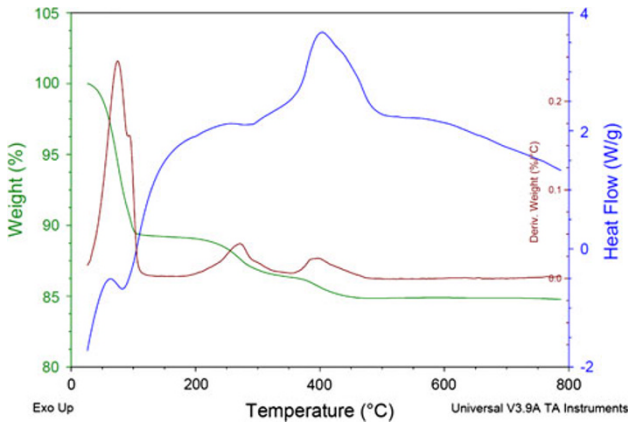

Fig. 1 DSC/TGA for precursor for ZnO

Experimental work

Materials

All chemicals used in this experiment having analytical grade purity were obtained from the commercial market, used without further any purification. For all the reactions, zinc acetate dihydrate $Zn(CH_3CO_2)_2{\cdot}2H_2O$, aluminum hydroxide acetate $AlOH(CH_3CO_2)_2$, and potassium hydroxide KOH were used for synthesis.

Calculated stoichiometric ratio of zinc acetate dihydrate $Zn(CH_3CO_2)_2{\cdot}2H_2O$ was taken in a beaker containing distilled water and stirred for 30 min. Potassium hydroxide KOH mixed in distilled water was added to the acetate solution. In case of Al-doped (3, 5, and 10%) ZnO nanomaterial different concentrations of aluminum hydroxide acetate $AlOH(CH_3CO_2)_2$ were added into the zinc solution before potassium hydroxide KOH solution. The reaction was stirred for 30 min at room temperature. When reaction was completed, we filtered the resultant white suspension using the centrifuge machine. Each centrifuge step had 5 min of rotation with the speed of 2,500 rpm. We obtained the white precipitates and then washed with distilled water and ethyl alcohol many times. The obtained white precipitates of zinc hydroxide/aluminum hydroxide were dried at

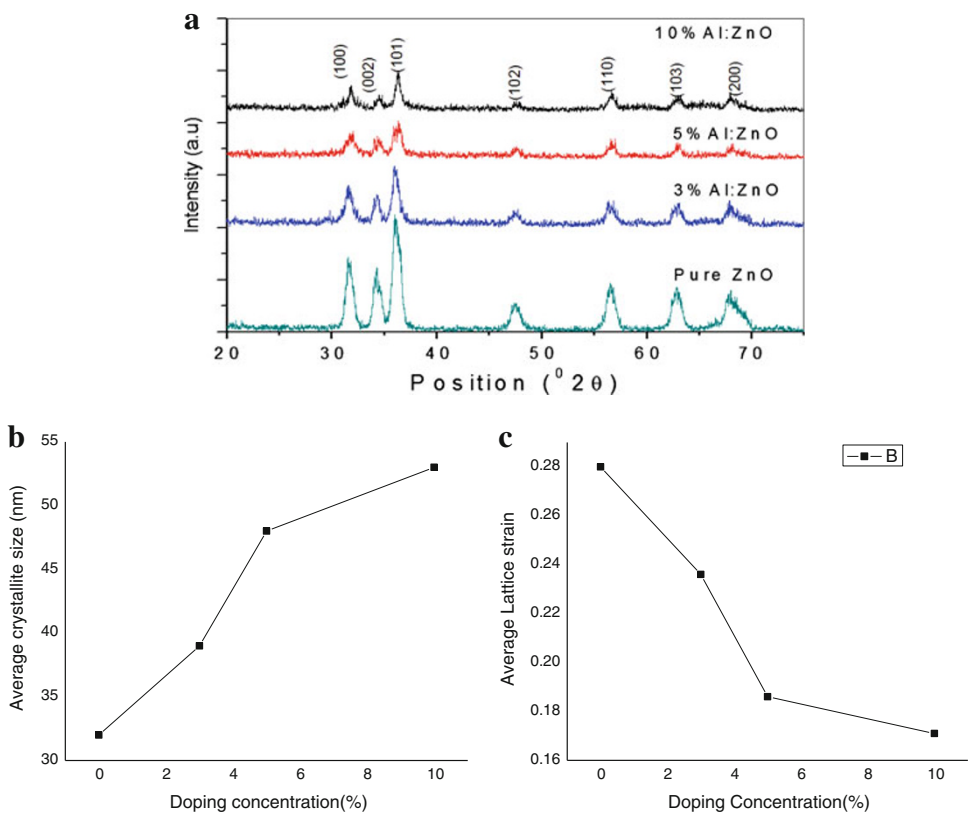

Fig. 2 **a** XRD pattern of ZnO/Al:ZnO nanomaterials. **b** Average crystallite size variation with doping concentration. **c** Average lattice strain variation with doping concentration

Table 2 X-ray investigation of the undoped and Al-doped ZnO

	ZnO				3% Al:ZnO				5% Al:ZnO				10% Al:ZnO			
Pos [2Th]	FWHM [2Th]	d-Spacing [A]	Crystallite size (nm)	Lattice strain	FWHM [2Th]	d-Spacing [A]	Crystallite size (nm)	Lattice strain	FWHM [2Th]	d-Spacing [A]	Crystallite size (nm)	Lattice strain	FWHM [2Th]	d-Spacing [A]	Crystallite size (nm)	Lattice strain
31.555	0.383	2.835	37	0.338	0.360	2.822	40	0.319	0.259	2.801	56	0.226	0.189	2.800	76	0.165
34.176	0.379	2.623	38	0.308	0.284	2.616	51	0.230	0.268	2.610	54	0.216	0.253	2.600	57	0.204
35.989	0.414	2.495	35	0.318	0.416	2.493	35	0.320	0.298	2.462	49	0.233	0.283	2.472	51	0.222
47.409	0.516	1.917	29	0.293	0.404	1.908	37	0.229	0.322	1.905	47	0.182	0.307	1.907	49	0.174
56.261	0.542	1.635	28	0.253	0.459	1.630	34	0.214	0.303	1.621	52	0.140	0.327	1.621	48	0.152
62.661	0.576	1.482	28	0.236	0.431	1.481	38	0.177	0.373	1.475	43	0.152	0.344	1.473	47	0.143
67.815	0.589	1.380	28	0.219	0.439	1.380	38	0.163	0.412	1.375	40	0.153	0.384	1.379	44	0.142

Table 3 Average crystallite size and lattice strain for ZnO/Al:ZnO nanomaterials

Sample	Average crystallite size (nm)	Average lattice strain
Pure ZnO	32	0.280
3% Al-doped ZnO	39	0.236
5% Al-doped ZnO	48	0.186
10% Al-doped ZnO	53	0.171

Table 4 Band gap for ZnO/Al:ZnO nanomaterials

Sample	Band gap E_g (eV)
Pure ZnO	3.01
3% Al-doped ZnO	2.99
5% Al-doped ZnO	2.97
10% Al-doped ZnO	2.94

60°C. Finally the thermal decomposition of zinc hydroxide/aluminum hydroxide was done to obtain the nanocrystals of ZnO and ZnAlO. We placed these zinc hydroxide and aluminum hydroxide in furnace chamber at 600°C for 1 h. The involved reactions are shown in Table 1.

Characterization of the product

Powder X-ray diffraction (XRD) data were recorded and collected on the XRD model MPD X'PERT PRO of PANalytical Company Ltd., Holland using Cu–Kα as characteristic radiation ($\lambda = 0.15418$ nm) with θ–θ configuration. The measurements were made in 2θ ranging from 20 to 70°. Study was mainly done by the software X'Pert HighScore of the same company. Scanning electron microscopy (SEM) images were taken on a scanning electron microscope (JEOL JSM-6480). A differential scanning calorimetery (DSC) and thermal thermogravimetric analyses (TGA) were performed by SDT Q600 of TA Instrument; the optical properties were investigated by ultraviolet–visible spectroscopy using UV/Vis spectrophotometer CECIL2700.

TGA and DSC analysis

To determine the thermal decomposition temperature of zinc hydroxide/aluminum hydroxide, differential scanning calorimetery (DSC) and thermal thermogravimetric analyses (TGA) were carried out by SDT Q600 of TA Instrument; the thermal decomposition curves (DSC/TGA) of zinc hydroxide/aluminum hydroxide are depicted in Fig. 1. The specimen was heated from room temperature to 800°C with an increment of 20°C/min in air. The TGA data plots the weight variation of the specimen, DSC designates whether reaction is endothermic or exothermic and weight derivative (temp) gives information about the rate of change of weight with respect to temperature.

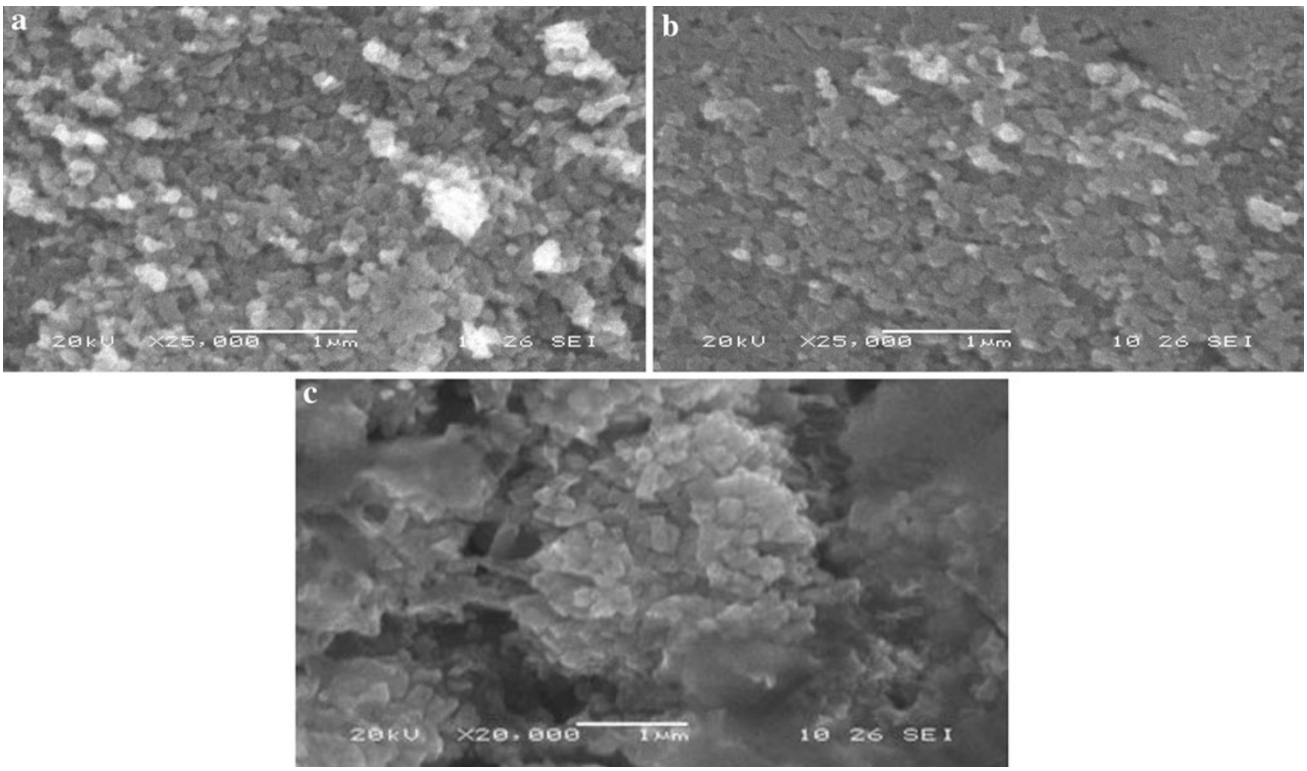

Fig. 3 **a** SEM image for ZnO nanomaterial. **b** SEM image for 3% Al:ZnO nanomaterial. **c** SEM image for 5% Al:ZnO nanomaterial

The specimen suffered the weight losses at 100 and 250°C, respectively, which is due to evaporation of ethyl alcohol, water, and organic by products. The evaporation is endothermic reaction; corresponding peaks emerge at DSC curve, weight derivative peaks also confirm the said conversion, we can observe another weight loss in TGA curve at 400°C, analogous large exothermic peak and weight derivative peaks are also exhibited at same temperature; due to the formation and crystallization of ZnO. Therefore, the crystallization of ZnO nanomaterial occurred at temperatures over 400°C. For this reason, we used 600°C for the thermal decomposition of prepared precursors.

Structural analysis

X-ray diffraction

Figure 2a shows the XRD patterns of ZnO/Al:ZnO nanomaterial annealed at 600°C for 1 h. All ZnO/Al:ZnO samples are polycrystalline and correspond to hexagonal structure that can be indexed by comparison with data from JCPDS file no. 03-065-3411 with lattice constants $a = 3.2495$ Å, $b = 3.2495$ Å, and $c = 5.2069$ Å. No diffraction peaks of Al_2O_3 or other impurities are observed, which show that the Al ions successfully reside in the lattice site rather than interstitial ones.

By comparing with undoped ZnO, the doped samples show lowering of intensity and decrease in full width at half maxima (FWHM). Average crystallite size calculated from XRD peaks is about 32 nm for undoped sample which goes up to 53 nm for the Al-doped samples.

We find the major diffraction peaks decreasing as the Al concentration increases, which indicates Al-doping effects and decreases the crystalline quality. Comparing the crystallization of ZnO with Al:ZnO, a large amount of Al dopants produce lattice disorder, which is linked with the reduction in lattice strain in ZnO. Moreover, the stain reduction, the grains grew much easier when Al dopants were included with ZnO.

To understand the crystalline mechanism of ZnO/Al:ZnO, the crystallite size of the ZnO/Al:ZnO nanomaterial has been estimated from the FWHM of diffraction peak using the Scherrer formula(Klug and Alexander 1974).

$$D = 0.9\lambda/\beta\cos\theta$$

where D is crystallite size, λ, θ, and β are the wavelengths of X-ray, the Bragg's diffraction angle and full width at half maximum (FWHM) of the diffraction peak, respectively. The graph between average crystallite size and doping concentration is shown in Fig. 2b.

The lattice strain (ε) has been determined by using the tangent formula (Klug and Alexander 1974). The graph

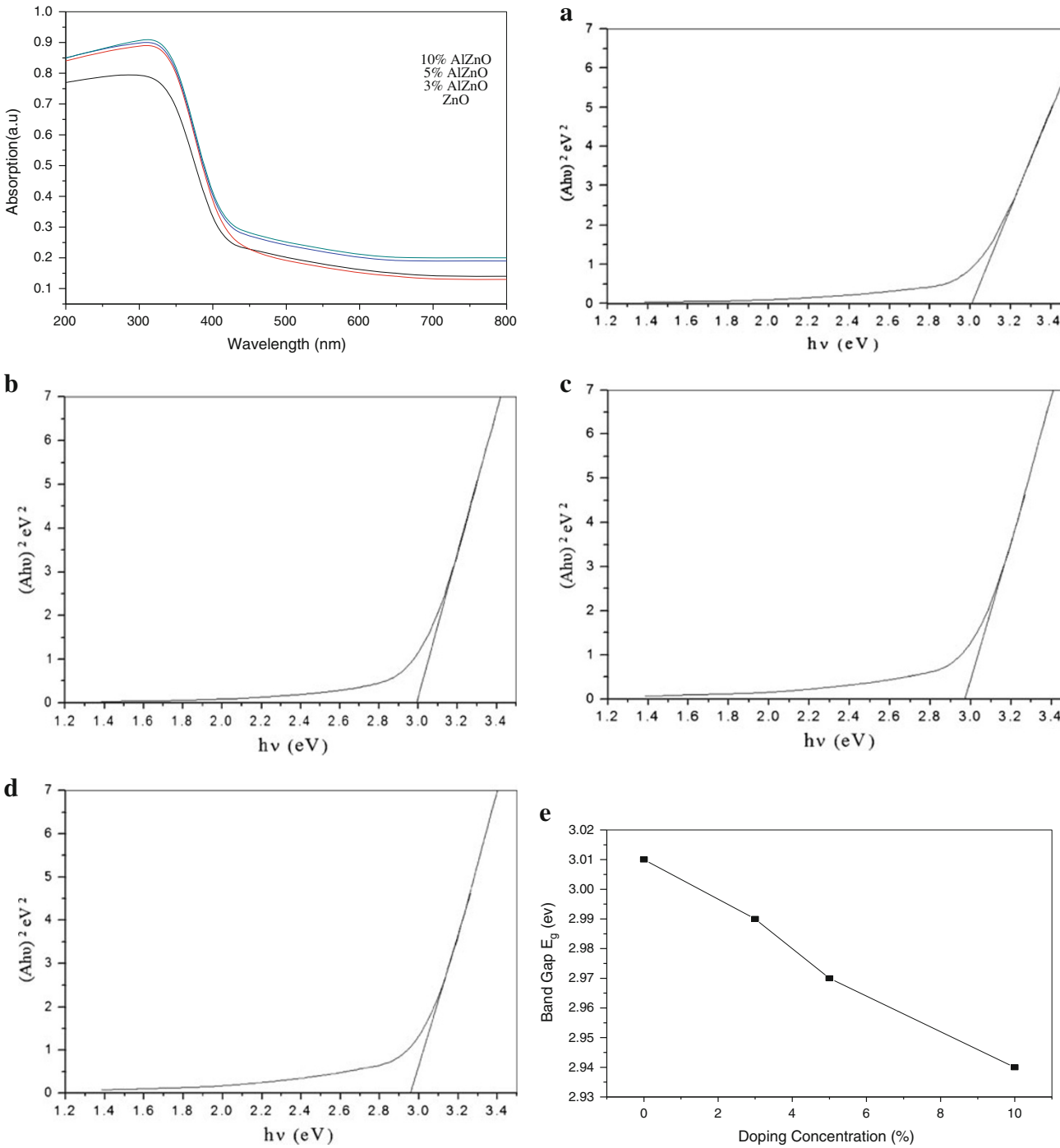

Fig. 4 Absorption spectrum of different samples in UV–visible region. **a** Band gap for pure ZnO nanoparticles. **b** Band gap for 3% Al:ZnO nanoparticles. **c** Band gap for 5% Al:ZnO nanoparticles. **d** Band gap for 10% Al:ZnO nanoparticles. **e** Band gap variation with doping concentration

between average lattice strain (ε_{av}) and doping concentration is shown in Fig. 2c.

$\varepsilon = \beta/(4\tan\theta)$.

The position (2θ), FWHM (β), crystallite size, and lattice strain of ZnO/Al:ZnO thus obtained are listed in Tables 2 and 3.

SEM results

The structural morphologies of the synthesized product were observed by the scanning electron microscopy model JSM 6480LV JEOL Japan. SEM images are collected at high magnifications to investigate the morphology of

samples. Figure 3a shows the SEM image for pure ZnO nanomaterial.

The magnification of this image is 25,000 times and reference bar of 1 μm. SEM micrograph shows that particles are random in shape with average particle size 125 nm, estimated by pixel analysis using ImageJ and Micro-Manager 1.4 softwares. Figure 3b, c show SEM images for 3 and 5% Al-doped ZnO nanomaterial, also having same magnification and reference bar, average particle sizes estimated are 150 and 176 nm, respectively. These SEM images show a narrow particle size distribution and particle size is growing as Al doping increases.

Optical analysis

Figure 4 shows the absorbance spectra of the undoped and Al-doped ZnO films for wavelength 200–800 nm The optical band gap (E_g), was estimated from the extrapolation of the linear portion in a plot of $(Ahv)^2$ against hv, where A is the absorbance and hv is the photon energy Table 4. It is observed that E_g in the undoped ZnO nanomaterial is ~3.01 eV which is lower than value of bulk ZnO (3.37 eV). This deviation may be due to the structural defects takes place at the time of synthesis and thermal treatment of precursor, On doping at 3% of Al, E_g is found to decrease to the 2.99 eV because of big crystallite size and small lattice strain as observed in the X-ray study. Further E_g decreases and becomes 2.97 and 2.94 eV, in the case of 5 and 10% Al doping, respectively. Similar type of E_g behavior have been reported by different researchers for sol–gel spin-coating to develop ZnO thin film(Natsume and Sakata 2000) and pulsed laser ablation (3.1 eV) (Narasimhan et al. 1999).

Figure 4a, b, c, d show the graph for the calculation of the band gap of undoped ZnO and doped ZnO with 3, 5, and 10% Al concentration. The graph between band gap and doping concentration is shown in Fig. 4e.

Conclusion

We have fabricated zinc oxide and aluminum-doped zinc oxide nanomaterial of different sizes. XRD data confirms the hexagonal phase of the synthesized materials. The crystallite size increases with increase in the doping concentration. The surface morphologies of the synthesized product were observed by the scanning electron microscopy (SEM). DSC/TGA analysis was done to study the phase changes during fabrication of materials. In DSC/TGA analysis it was found that $Zn(OH)_2/Al(OH)_3$ decompose to form the required product. A spectrophotometer was used to attain the absorption spectrum in ultraviolet–visible region. It was found that absorption is maximum for highest doping and band gap of the materials was also calculated.

Acknowledgments The authors acknowledge Higher Education Commission, Pakistan for financial support through "Indigenous Ph.D. Fellowship Program (5000 Fellowships)".

References

Alhamed M, Abdullah W (2010) Structural and optical properties of ZnO:Al films prepared by the sol–gel method. J Electron Devices 7:246–252

Ananthakumar S, Anas S, Ambily J, Mangalaraja RV (2010) Microwave assisted citrate gel combustion synthesis of ZnO part-II: assessment of functional properties. J Ceram Process Res 11(2):164–169

Bandyopadhyay S, Paul GK, Sen SK (2002) Study of optical properties of some sol–gel derived films of ZnO. Sol Energy Mater Sol Cells 71:103–113

Chen JJ, Yu MH, Zhou WL, Sun K, Wang LM (2005) Room-temperature ferromagnetic Co-doped ZnO nanoneedle array prepared by pulsed laser deposition. Appl Phys Lett 87:173119

Dixit H, Saniz R, Lamoen D, Partoens B (2011) Accurate pseudo-potential description of the GW bandstructure of ZnO. Comp Phys Comm 182:2029

Fons P, Tampo H, Kolobov AV, Ohkubo M, Niki S, Tominaga J, Carboni R, Friedrich S (2006) Direct observation of nitrogen location in molecular beam epitaxy grown nitrogen-doped ZnO. Phys Rev Lett 96:045504

Fortunato E, Barquinha P, Pimentel A, Goncalves A, Marques A, Pereira L, Martins R (2005) Recent advances in ZnO transparent thin film transistors. Thin Solid Films 487:205–211

Friedrich C, Müller MC, Blügel S (2011) Band convergence and linearization error correction of all-electron GW calculations: the extreme case of zinc oxide. Phys Rev B 83:081101 (R)

Gong H, Hu JQ, Wang JH, Ong CH, Zhu FR, Sens (2006) Nano-crystalline Cu-doped ZnO thin film gas sensor for CO. Actuators B 115:247–251

Inamdar AI, Mujawar SH, Patil PS (2007) The influences of complexing agents on growth of zinc oxide thin films from zinc acetate bath and associated kinetic parameters. Int J Electrochem Sci 2:797–808

Jeong IS, Kim JH, Im S (2003) Ultraviolet-enhanced photodiode employing *n*-ZnO/*p*-Si structure. Appl Phys Lett 83:2946–2948

Joseph B, Gopchandran KG, Thomas PV, Koshy P, Vaidyan VK (1999) A study on the chemical spray deposition of zinc oxide thin films and their structural and electrical properties. Mater Chem Phys 58:71–77

Klug HP, Alexander LE (1974) X-ray diffraction procedures for polycrystalline and amorphous materials. Wiley, NewYork

Kuo SY, Chen WC, Cheng CP (2006) Investigation of annealing-treatment on the optical and electrical properties of sol–gel-derived zinc oxide thin films. Superlattices Microstruct 39:162–170

Ma S, Liang H, Wang X, Zhou J, Li L, Sun CQ (2011) Controlling the band gap of ZnO by programmable annealing. J Phys Chem C 115:20487–20490

Makino T, Chia CH, Nguen TT, Segawa Y (2000) Radiative and nonradiative recombination processes in lattice-matched (Cd, Zn)O/(Mg, Zn)O multiquantum wells. Appl Phys Lett 77:1632–1634

Muscat J, Wander A, Harrison NM (2001) On the predivction of band gaps from hybrid density-functional theory. Chem Phys Lett 342:397

Narasimhan KL, Pai SP, Palkar VR, Pinto R (1999) High quality zinc oxide films by pulsed laser ablation. Thin Solid Films 295:104

Natsume Y, Sakata H (2000) Zinc oxide films prepared by sol–gel spin-coating. Thin Solid Films 372:30

Oshikiri M, Aryasetiawan F (2000) Quasiparticle Energy Calculations on II(Zn)-VI(O, S, Se) and III(Al, Ga)-V(N) Semiconductors in the Wurtzite Structure. J Phys Soc Jpn 69:2113–2120

Park JH, Jang SJ, Kim SS, Lee BT (2006) Growth and characterization of single crystal ZnO thin films using inductively coupled plasma metal organic chemical vapor deposition. Appl Phys Lett 89:121108

R. F Service (1997) Materials science: will UV lasers beat the blues? Science 276:895

Ristic M, Music S, Ivanda M, Popovic S (2005) Sol–gel synthesis and characterization of nanocrystalline ZnO powders. J Alloys Compd 397:L1–L4

Sakthivelu A, Saravanan V, Anusuya M, Joseph Prince J (2011) Structural, morphological and optical studies of molarity based ZnO thin films. J Ovonic Res 7(1):1–7

Shishkin M, Kresse G (2007) Self-consistent GW calculations for semiconductors and insulators. Phys Rev B 75:235102

Song J, Zhou J, Wang ZL (2006) Piezoelectric and semiconducting coupled power generating process of a single ZnO belt/wire. A technology for harvesting electricity from the environment. Nano Lett 6:1656–1662

Tan ST, Chen BJ, Sun XW, Fan WJ (2005) Blueshift of optical band gap in ZnO thin films grown by metal-organic chemical-vapor deposition. J Appl Phys 98:013505

Uddin J, Scuseria GE (2006) Theoretical study of ZnO phases using a screened hybrid density functional. Phys Rev B 74:245115

Usuda M, Hamada N (2002) All-electron GW calculation based on the LAPW method: application to wurtzite ZnO. Phys Rev B 66:125101

Yan Q, Rinke P, Winkelnkemper M, Qteish A, Bimberg D, Scheffler M, Van deWalle CG (2011) Band parameters and strain effects in ZnO and group-III nitrides. Semicond Sci Technol 26:014037

Yu ZG, Wu P, Gong H (2006) Control of p- and n-type conductivities in P doped ZnO thin films by using radio-frequency sputtering. Appl Phys Lett 88:132114

Zandi S, Kameli P, Salamati H, Ahmad H, Hakimi M (2011) Microstructure and optical properties of ZnO nanoparticles prepared by a simple method. Phys B 406:3215–3218

Zhang ZZ, Lu YM, Shen DZ, Yao B, Zhang JY, Li BH, Zhao DX, Fan XW, Tang ZK (2006) ZnO *p–n* junction light-emitting diodes fabricated on sapphire substrates. Appl Phys Lett 88:031911